Ion Density Climatology Based on FPMU Measurements on Board the International Space Station

Sophia R. Laranja[1,2], Bela G. Fejer[3], Marco A. Ridenti[1], J. Amorim[1], and Charles M. Swenson[2]

[1]Space Sciences Laboratory, Aeronautics Institute of Technology, São José dos Campos, SP, BRA
[2]Department of Electrical and Computer Engineering, Utah State University, Logan, UT, USA
[3]Center for Atmospheric and Space Sciences, Utah State University, Logan, UT, USA

Key Points:

- The FPMU daytime densities are generally in good agreement with the results from the International Reference Ionosphere (IRI)
- A bulge in the EIA southern crest possibly associated with the Weddell Sea anomaly (WSA) was observed during the daytime
- Two midlatitude summer nighttime anomalies (MSNAs) were observed until the early morning and were stronger in a higher solar flux period

Corresponding author: S. R. Laranja, sophiasrl@ita.br

Abstract

We performed, for the first time, a season-dependent geomagnetically quiet-time climatology of mid- and low-latitude ion densities during low and moderate solar flux conditions using Floating Potential Measurement Unit (FPMU) observations aboard the International Space Station (ISS) from 2008 to 2019. Our daytime observations indicate that the main characteristics of the equatorial ionization anomaly (EIA) at ∼400 km are consistent with those from other in-situ and remote sensing probes. The FPMU daytime densities are also generally in good agreement with the corresponding results from the International Reference Ionosphere (IRI). However, the IRI does not reproduce the mid-solar flux evening low-latitude measured densities. In this period, the EIA exhibits strong longitude-dependent crest-to-trough ratios and asymmetries due to the pre-reversal enhancement (PRE) of the zonal electric field and thermospheric neutral winds. Our data also show strong structuring of the daytime and nighttime plasma densities. This includes a bulge, discussed for the first time here, in the EIA southern crest in the South Atlantic sector during the December solstice and equinox data, which we suggest being generated by the transport of plasma from the Weddell Sea anomaly (WSA). We also highlight and show the evolution of a midlatitude summer nighttime anomaly (MSNA) during the June solstice data in the North Atlantic sector. Our results give new insights into these two anomalies, where we show that they are stronger with increasing solar flux levels and that they last until the early morning. These latter results are not consistent with those from previous studies.

1 Introduction

The ionosphere at low latitudes is site of several phenomena driven by complex interactions between atmospheric, ionospheric, and magnetospheric processes mediated by the magnetic and gravitational fields (Kelley, 2009; Rishbeth & Garriott, 1969). The Equatorial Ionization Anomaly (EIA) (Appleton, 1946), characterized by plasma density minima near the magnetic equator and maxima at magnetic latitudes of about ±15°, is the most prominent feature of the daytime low latitude F-region ionosphere. The EIA results from plasma flow along the field lines driven by the effects of the field-perpendicular $E \times B$ upward plasma motion and field-aligned diffusion (Balan et al., 2018a). The strength, location, and asymmetry of the EIA density crests vary with longitude, season, and solar cycle due mostly to the corresponding variations of the equatorial vertical plasma drifts (e.g., Fejer, 2011; Fejer & Maute, 2021) and magnetic meridional winds (e.g., Balan et al., 2008, 2018b). In the early night period, the evening pre-reversal enhancement (PRE) of the equatorial upward drifts plays a major role in the strong season, solar cycle, and longitude-dependent low latitude F-region plasma density distribution and irregularity occurrence (e.g., Heelis et al., 1974; Rishbeth, 1981).

Large latitude and longitude-dependent F-region plasma density gradients associated with vertical plasma drifts and neutral winds have long been known (e.g., Hanson & Sanatani, 1971; Wharton et al., 1980). Latitudinal density asymmetries result from differences in field-aligned ion motions and F-layer height driven by imbalanced magnetic meridional winds on both sides of the magnetic equator (Balan et al., 1997a; Bailey et al., 2000). Simulations presented by Luan and Solomon (2008) indicated that most of the magnetic meridional winds' longitudinal variations result from zonal wind and magnetic declination effects. Asymmetric meridional winds give rise to stronger crests in the hemisphere of the equatorward flow where chemical loss and downward diffusion are reduced due to the F-layer rise (Balan et al., 2008; Batista et al., 2011).

Low Earth Orbit (LEO) satellites have yielded extensive global information on low- and mid-latitude ionospheric density distribution. J.-Y. Liu et al. (2022) discussed the characteristics of plasma depletion bays and the Weddell Sea density anomaly observed by the FORMOSAT-3/COSMIC (F3/C) satellite constellation. Plasma depletion bays

(PDBs) are broad regions of low nighttime plasma density in the low latitude winter hemisphere that extend to the summer hemisphere of generally high densities (F.-Y. Chang et al., 2020). The Weddell Sea anomaly (WSA), centered near (73°S, 45°W) in Antarctica's Weddell Sea region, exhibits the unusual pattern of higher summer plasma densities during nighttime compared to daytime (Penndorf, 1965). Burns et al. (2008) used COSMIC data to hypothesize that an evening downward plasma flux from the plasmasphere may contribute to this phenomenon. Lin et al. (2009) used F3/C electron density measurements to suggest that the poleward offset of the magnetic equator from the geographic equator is important in its formation. On the other hand, L. C. Chang et al. (2015) used HWM93 (Horizontal Wind Model) to demonstrate that equatorward and upward neutral wind effects are essential in the WSA development. The WSA is part of the midlatitude summer nighttime anomalies (MSNAs), all of which exhibit the same formation mechanisms (e.g., Chen et al., 2012; Lin et al., 2009, 2010; H. Liu et al., 2010) described earlier.

The Floating Potential Measurement Unit (FPMU) on board the International Space Station (ISS) has been making plasma density and electron temperature measurements since 2006. Most of these data have been used only for validation purposes under different geophysical conditions (Barjatya et al., 2009; Coffey et al., 2008; Debchoudhury et al., 2021; Hartman et al., 2019). Recently, FPMU data has also been used for studying morning electron temperature overshoots (Yang et al., 2020), and nighttime O^+ dropouts (Debchoudhury et al., 2022). In addition, Newheart et al. (2022) used a few days of FPMU and SWARM spacecraft ionospheric densities along with Total Electron Content (TEC) observations to examine well-defined EIAs around local midnight during geomagnetically quiet periods.

We use FPMU measurements from 2008 to 2019 for the first comprehensive study of the seasonal and solar cycle-dependent quiet time mid- and low-latitude F region climatology and large-scale structures at ∼400 km. We will focus on the evolution of evening and nighttime low-latitude ionospheric structures during moderate solar activity and magnetically quiet conditions. In the following sections we first briefly describe our data and then proceed to present and discuss our results. The Supporting Information presents all the figures in a colorblind-friendly format.

2 Measurements and Data Analysis

The Floating Potential Measurement Unit (FPMU) was developed with the primary purpose of studying the surface charging of the ISS (Barjatya et al., 2009). The ISS operates at an altitude varying from about 380 to 420 km with an orbital inclination of 51.6° and an orbital period of 92 min, corresponding to ∼16 orbits per day. The FPMU consists of a suite of four instruments (Wide Langmuir Probe, Narrow Langmuir Probe, Floating Potential Probe, and Plasma Impedance Probe) providing 1-s measurements of the ISS frame potential and in-situ plasma densities and electron temperatures (Barjatya et al., 2009). FPMU-derived ion densities and electron temperatures are available at the NASA Space Physics Data Facility (SPDF) Coordinated Data Analysis Web (CDAWeb) website, `https://cdaweb.gsfc.nasa.gov`. Very little data is available from 40°E-90°E due to limited communications between the ISS and ground stations.

We used FPMU plasma densities measured during magnetically quiet periods (Kp < 3) from December 2008 to December 2019. This period encompasses the Solar Cycle 24, which was mostly characterized by low solar activity. Our data was divided into low ($\Phi < 100$ sfu, solar flux unit $= 10^{-22}$ W m^{-2} Hz^{-1}) and moderate ($\Phi > 100$ sfu) solar flux levels, with mean values of 75 and 130 sfu, respectively; and three seasons: December solstice (November-February), equinox (March, April, September, and October), and June solstice (May-August). The plasma densities were first averaged in each bin of a $5° \times 5°$ grid covering latitudes up to $\pm 50°$ and then smoothed using a Savitzky-Golay

filter (Savitzky & Golay, 1964) with a 9° longitude window length and a second-degree polynomial along each latitude.

3 Results and Discussion

3.1 Ionospheric Density Climatology at the ISS height

Figures 1-3 present climatologies of afternoon and evening mid- and low-latitude plasma densities at about 400 km measured by FPMU from 2008 to 2019 during the December solstice, equinox, and June solstice, respectively. These figures show the largest densities at 14:00-16:00 LT (panels c-d) and decreasing values toward the night. In general, the peak densities increase from about 10^6 cm^{-3} during low solar flux to about 2.5 $\times$ 10^6 cm^{-3} during moderate solar flux conditions, while the anomaly crests remain at about the same geomagnetic latitudes until ∼14:00 LT. Later, the low solar flux anomaly significantly weakens with time and essentially disappears close to sunset, while under moderate solar flux conditions, the anomaly intensifies towards sunset with crests further poleward and increasing crest-to-trough density ratios. This is readily explained by the transport of plasma to higher equatorial altitudes and geomagnetic latitudes in response to the increase of late afternoon and evening upward plasma drifts with solar flux (Fejer, 1991; Fejer et al., 2008).

Our solstice data (Figures 1 and 3) show that the winter hemisphere crests tend to be closer to the dip equator than the summer hemisphere crests, as reported earlier (e.g., Cai et al., 2020; Khadka et al., 2018; Xiong et al., 2013). This was attributed to the upward and downward shifting of the anomaly crests driven by the meridional neutral winds. The neutral wind effect is also responsible for the greater densities seen in the summer hemisphere crests. In contrast to the result by Luan et al. (2015), our data show that this solstitial asymmetry is more evident for low solar flux conditions. On the other hand, the absence of a clear southern crest during the June solstice in both flux levels of Figure 3 indicates a weaker solar flux effect on the EIA response to the thermospheric wind. Additionally, Figure 1 indicates that the December solstice EIA crest latitude separation is smaller in the region of large magnetic declination, i.e., roughly from Eastern Asia to Western South America, consistent with the study of Eastes et al. (2023). This is especially true during the evening. Furthermore, the December solstice densities are greater than the June solstice. This is the so-called annual asymmetry, consistent with previous studies (e.g., Burns et al., 2012; Zeng et al., 2008).

The equinox exhibits the most dramatic density changes with solar flux. The low flux panels in Figure 2 indicate that the northern EIA crest is, in general, stronger and at higher latitudes than the southern until 16:00 LT. During the evening, the separation between the two crests is not evident, but instead, the EIA appears as a single peak at the dip equator. The crests are possibly at a lower altitude given that the corresponding PRE amplitude is reduced in a low solar flux (Batista et al., 2011). Additionally, there is an intrinsic 4-wave modulation in the evening EIA which we associate with the wavenumber-4 (WN4) longitudinal structure (e.g., Lin et al., 2007; Wan et al., 2008). The longitudinal structure shown in Figures 2a, c, e, and g has density peaks in the Pacific, South American, African, and Eastern Asian sectors, in agreement with solar minimum ion density measurements presented by Choi et al. (2023). The vertical $E \times B$ drift, which is generally associated with the WN4, is the most effective driver of this structure in the daytime (Bankov et al., 2009; Fejer et al., 2008).

In contrast to the generally single density peak at the magnetic equator during equinoctial low flux conditions, the evening and early night EIA is symmetric around the dip equator during equinoctial moderate flux conditions, as illustrated in Figures 2f and 2h. In the equinox, the meridional wind effect is minimal compared to that during solstices due to a weaker pressure gradient between the two hemispheres (Cai et al., 2020; Huang

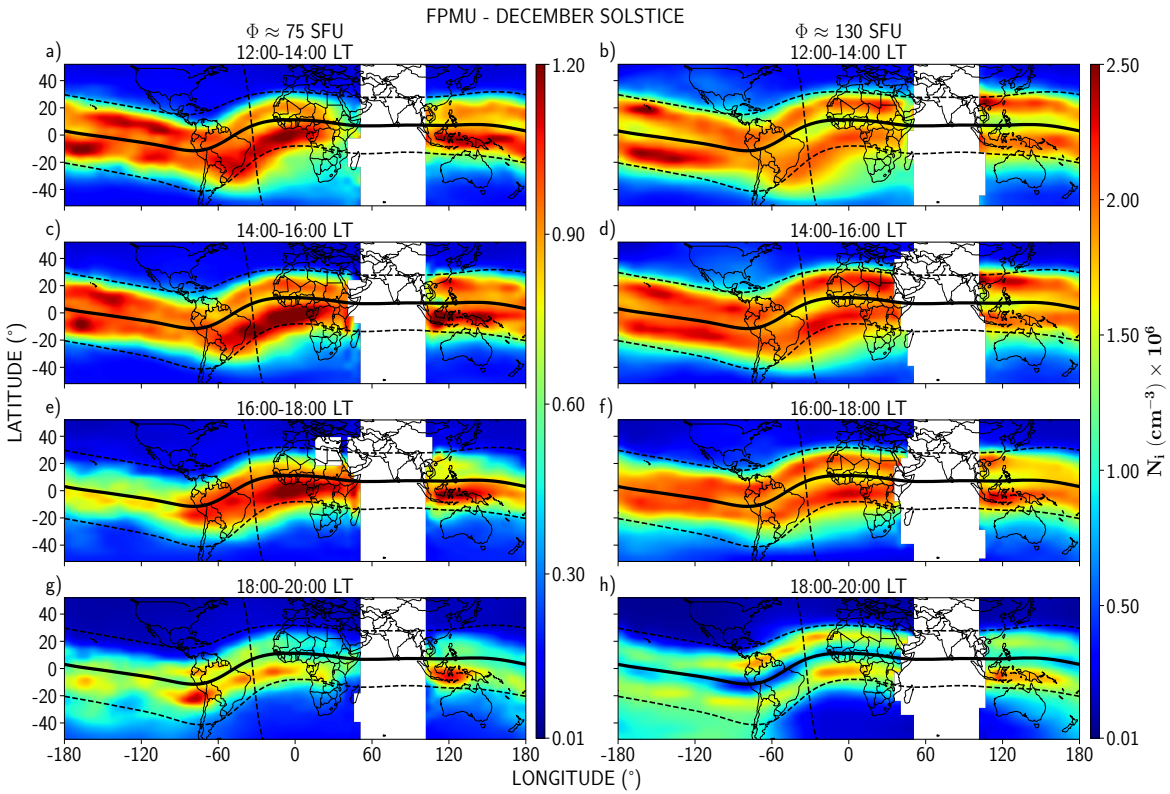

Figure 1. Middle and low latitude average December solstice plasma densities measured by the FPMU for low (left panels) and moderate (right panels) levels of solar activity. The solid black line is the magnetic dip equator and the dashed black lines represent the dip latitudes of ±20° and the 40° magnetic longitude.

et al., 2010). Balan et al. (2013) and Tulasi Ram et al. (2009) stated that zonal winds have a continuous and substantial influence throughout the equinox. Indeed, a wave-4 pattern exists in the evening ion density for the low flux, demonstrating the small effect of the meridional winds. Our data at the ISS height show the greatest densities during the equinox, illustrating the so-called semi-annual density variation (e.g., Balan et al., 1997b, 1998; Burns et al., 2012). Balan et al. (1997b) and Balan et al. (1998) attribute this variation to solar zenith angle, thermospheric composition, and equinox-neutral winds, influencing chemical and dynamical processes. As indicated above, the EIA displays symmetric crests' latitudes and densities only during the equinoxes, which is in accordance with the comprehensive study by Xiong et al. (2013).

The June solstice data also displays a wavelike density modulation. This can be seen in Figures 3a, c, and e where there is a 3-wave longitudinal modulation from 12:00 to 18:00 LT in the northern EIA crest. A similar wave-3 pattern in the northern summer was found by Huang et al. (2010) and by H. Liu et al. (2010), who also observed it at 12:00 LT. Moreover, our low and moderate June solstice data show plasma depletions in the South American sector northern crest at 18:00-20:00 LT, which are more pronounced for low solar flux conditions. We associate these structures to a plasma depletion bay, although seen at later local times in previous studies (e.g., J.-Y. Liu et al., 2022).

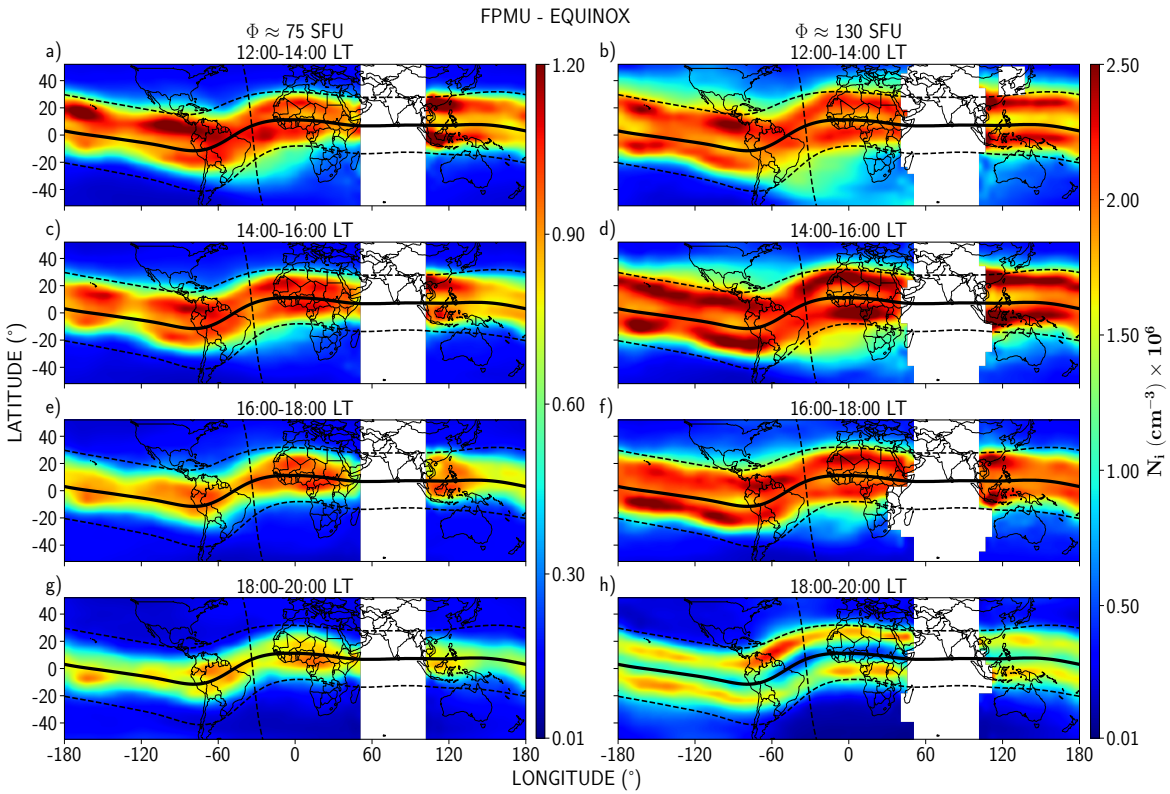

Figure 2. Same as Figure 1, but for the equinox.

3.2 Comparison with IRI-2020

We compared the FPMU climatology shown in Figures 1-3 with corresponding results from IRI version 2020 (Bilitza et al., 2022), which is available for download at `https://irimodel.org/`. We observed generally a very good agreement between the IRI and the FPMU daytime plasma densities at about 400 km, although the model slightly overestimates the densities during low solar flux conditions and underestimates them for moderate conditions. The largest variations were observed for moderate solar flux near dusk at low latitudes. Therefore, we focus on results only during these conditions.

Figure 4 illustrates that the IRI strongly underestimates the moderate solar flux evening and early night FPMU densities. In particular, the well-defined EIA crests are not seen in any season in the IRI data. The IRI densities are higher in the summer hemisphere, but they are much smaller than the corresponding FPMU values. The largest discrepancies are observed during the equinox where the symmetric crests shown in the data are not reproduced by the model. The main differences shown in Figure 4 can be attributed to the IRI's use of monthly averages and its mid-latitude main data sources (Bilitza et al., 2022), leading to better performance there compared to low-latitudes and the smoothing of evening and early night PRE effects, which play a major role in the anomaly generation. We note that the PRE increases with solar flux and is generally strongest during equinox (e.g., Scherliess & Fejer, 1999). We proceed to examine this effect in more detail.

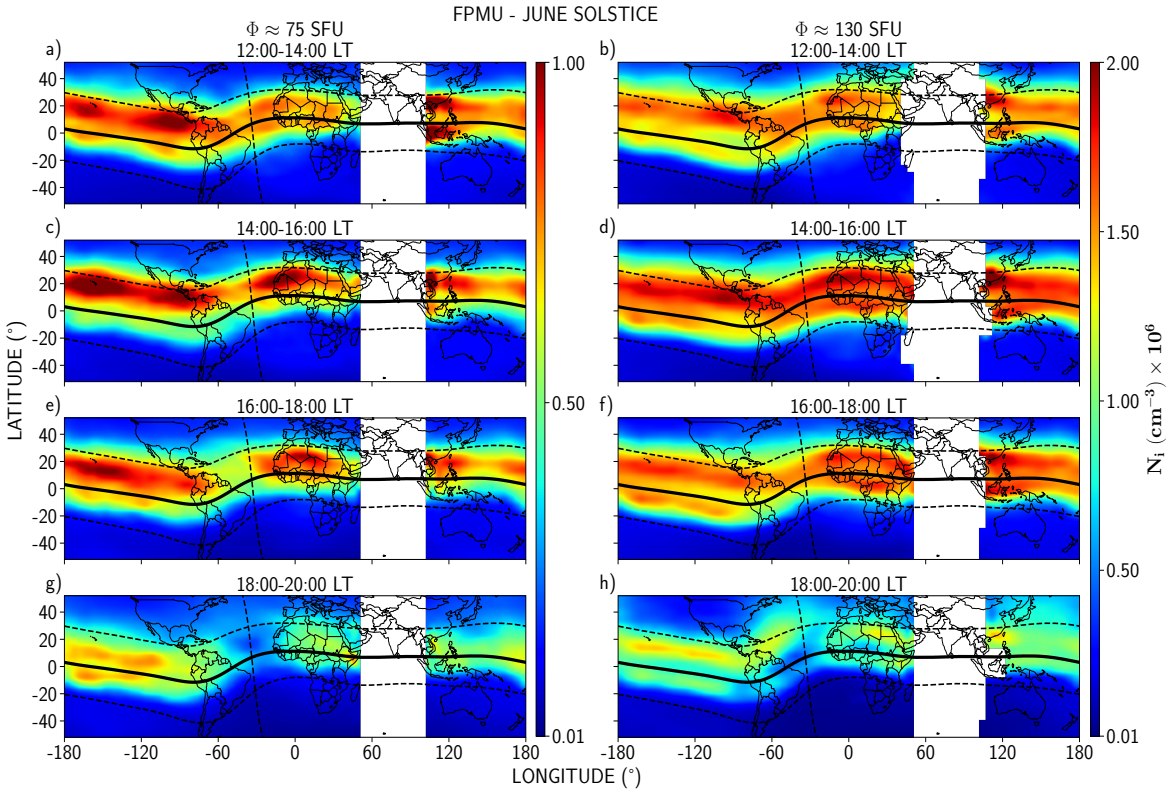

Figure 3. Same as Figure 1, but for the June solstice.

3.3 Evening results

Figure 5 shows the FPMU densities at 18:00-20:00 LT and 20:00-22:00 LT for $\Phi \approx$ 130 sfu, along with the peak values of the evening vertical plasma drift velocity (PRE peak) and their time-integrated (integrated PRE) values. These parameters were retrieved from Stolle et al. (2008) and obtained from ROCSAT-1 (Republic of China Satellite 1) measurements (Fejer et al., 2008). The integrated PRE values were obtained by summing the vertical drift values at each local time and multiplying them by the time difference between adjacent local time bins, therefore its unit is length. For the PRE peak, Stolle et al. (2008) used the highest drift value between 17:00 and 21:00 LT at each longitude for each season. The PRE is season- and longitude-dependent and is strongest when the sunset terminator and magnetic field lines are aligned (Abdu et al., 1981). It peaks between about 18:30 LT and 19:30 LT and affects the F-region plasma densities in approximately half the typical daytime response time of 3-4 hours, as shown by extensive VTEC (Vertical Total Electron Content) and airglow observations (Kumar et al., 2021).

Figure 5 shows that during the December solstice, the PRE and its integrated value are maximum at approximately -45° longitude, coinciding with the location where the EIA crests density increase and have the greatest latitudinal separation. During the equinox, the PRE and its integrated value peak around -100° and 0° longitudes but have little longitudinal variation. In this case, the strongest plasma densities in the anomaly occur at about 10° further east, which is consistent with the evening eastward motion of the F-region plasma (e.g., Fejer & Maute, 2021). During the June solstice, the PRE peak and integrated PRE are both close to zero in the South American and South Atlantic sectors, concordant with the absence of the EIA. These results are consistent with ear-

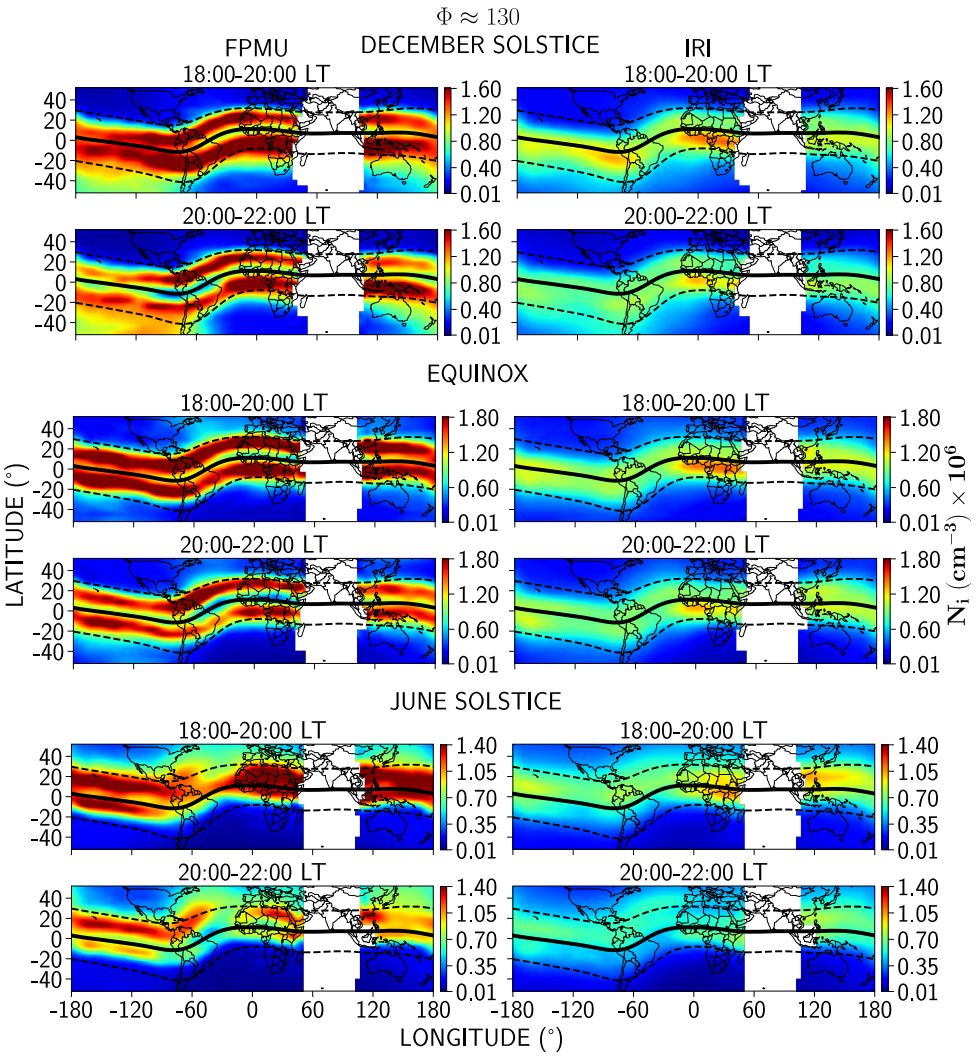

Figure 4. FPMU (left panels) and IRI-2020 (right panels) moderate solar flux evening and early night plasma densities.

lier studies indicating that the longitudinal distribution of the evening and nighttime anomaly is determined primarily by the PRE (e.g., Li et al., 2008; Whalen, 2004). We have considered moderate solar flux conditions only; however, evening vertical drifts can strongly affect nighttime ambient low-latitude F region electron density also for solar minimum conditions (e.g., Dao et al., 2011). As mentioned earlier, neutral winds also play important roles in the morphology of the anomaly. In addition, the north-south crest asymmetry is also affected by ambipolar diffusion from high and subauroral latitude ionosphere (J. Liu et al., 2016), displacement of the geographic and geomagnetic equators (Balan et al., 2013; Khadka et al., 2018; Zeng et al., 2008), and by the distance of the subsolar point to the magnetic equator (Eastes et al., 2023).

3.4 Plasma Density Structure in the Atlantic and American Sectors

The FPMU climatologies presented above illustrate the occurrence of strong daytime and nighttime plasma density structures or so-called anomalies. We now proceed to examine them in detail focusing on the Atlantic and American sectors.

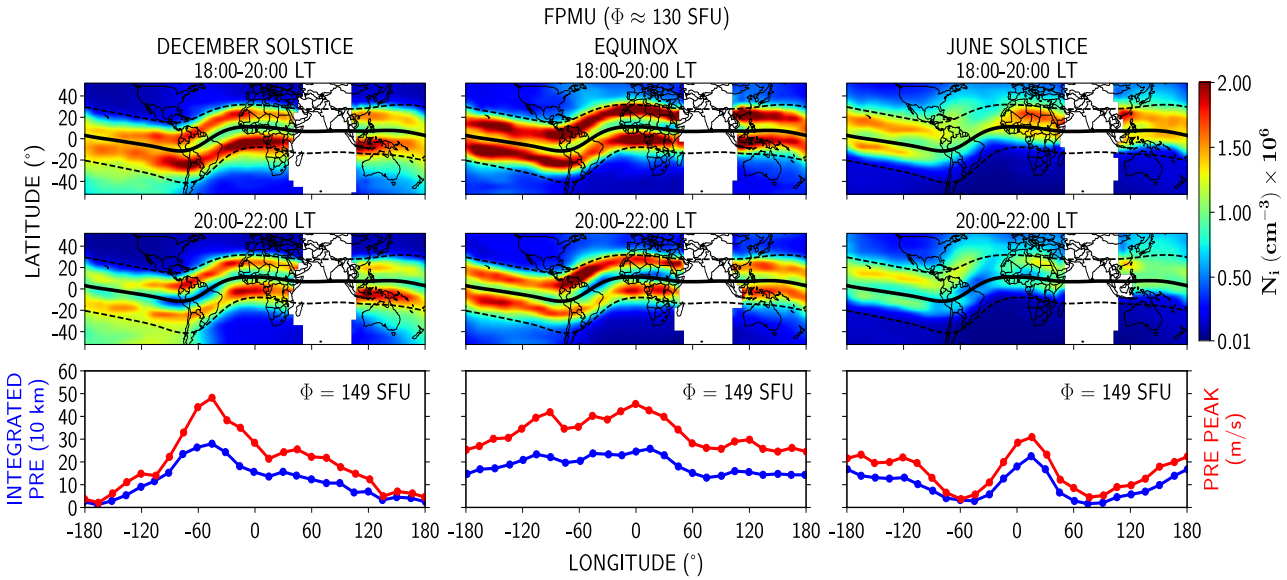

Figure 5. Upper panels. FPMU evening average plasma densities. Lower panels. Peak PRE plasma drifts and their time-integrated values in units of 10 km (adapted from Stolle et al., 2008).

3.4.1 Midlatitude Summer Nighttime Anomalies

Figures 6-8 show nighttime average FPMU plasma densities in the 95°W-15°E longitude sector. These figures illustrate the midlatitude summer nighttime anomalies, which here encompass the Weddell Sea anomaly and the nighttime June solstice density enhancement, for low (left panels) and moderate (right panels) solar flux conditions. We will now present their season-dependent characteristics at the ISS altitude.

December solstice. The enhanced plasma densities in the far southward-displaced southern EIA crest at the 20:00 LT December solstice panels (Figures 6c-d) appear to give rise to the Weddell Sea anomaly by 22:00 LT (Figures 6e-f). In our flux levels and ISS height, this anomaly is centered at South Pacific and South American longitudes until 02:00 LT, when it moves eastward until the early morning. It is stronger and concentrated to the north for moderate solar flux. In a broader perspective, the WSA is merged with the EIA southern crest. Additionally, the shape and location of the plasma excursion from the EIA southern crest suggest a strong connection with the excursion of the magnetic dip equator into the southern hemisphere.

June solstice. In this season, Figure 8 shows density peak structures along the 20° dip latitude line in the North Atlantic sector. These are the above-mentioned nighttime June solstice density enhancement or North Atlantic MSNA. For $\Phi \approx 130$ sfu, this anomaly starts between 18:00 and 20:00 LT (Figure 8b) as a density bulge in the northern EIA crest, developing into a tongue-like shape at 20:00-22:00 LT. At 22:00-24:00 LT (Figure 8f), the structure is now displaced to the east and to the north, following the tilt of the 20° dip latitude line. Although the density decreases over the nighttime hours, the structure still retains the highest plasma density in the middle and low-latitude ionosphere.

The June solstice low flux density anomaly shown in the left panels of Figure 8 starts at 20:00-22:00 LT, which is later compared to the moderate flux case. During most of the nighttime, it displays the same behavior as at the higher flux level, but with a lower

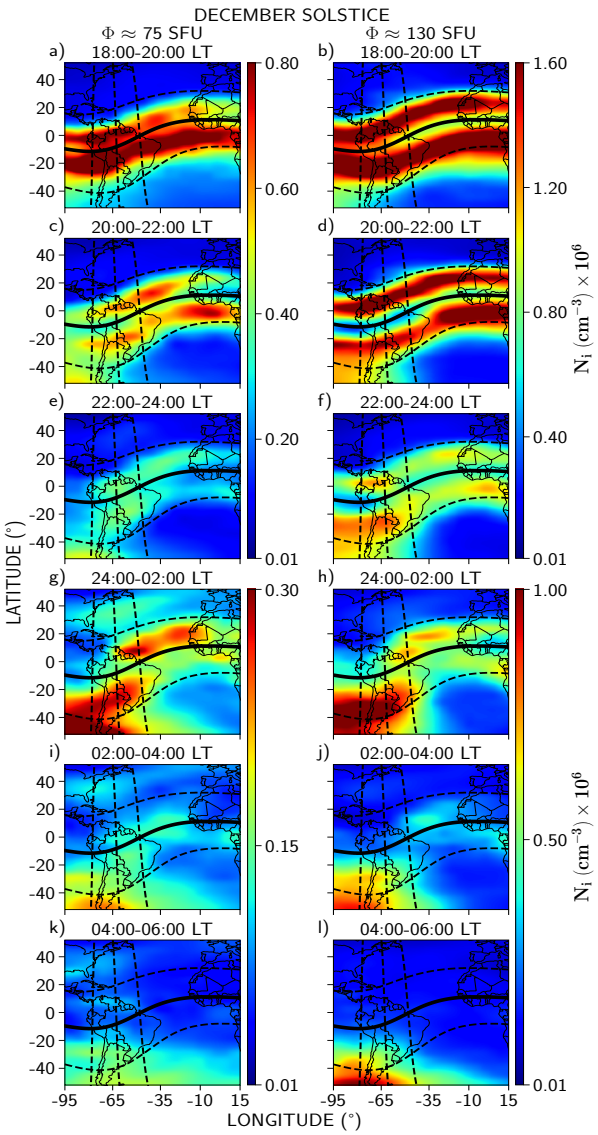

Figure 6. FPMU-measured December solstice plasma density in the 95°W-15°E longitude sector in low (left panels) and moderate (right panels) solar flux conditions. The solid black line denotes the magnetic dip equator and the dashed gray lines correspond, from left to right, to the -5°, 10°, and 25° magnetic longitudes.

area and density. At 02:00-04:00 LT (Figure 8i), the anomaly moves north of the 20° dip latitude line and maintains this pattern until the early morning. From 06:00 LT, the North Atlantic MSNA is no longer seen (not shown here).

We can also notice the evolution of the June solstice anomaly by following the three dashed gray lines in Figure 8, which correspond to the -5°, 10°, and 25° magnetic longitudes. The anomaly holds until ∼02:00 LT and then slowly decreases due to the weakening of the EIA during post-midnight hours, but it can be clearly observed until 06:00 LT. Albeit not clear in Figure 8, the anomaly is accompanied by a decrease in the plasma density at the conjugate location in the southern hemisphere. In contrast to the low solar flux case, in the right panels of Figure 8, the North Atlantic MSNA is observed at

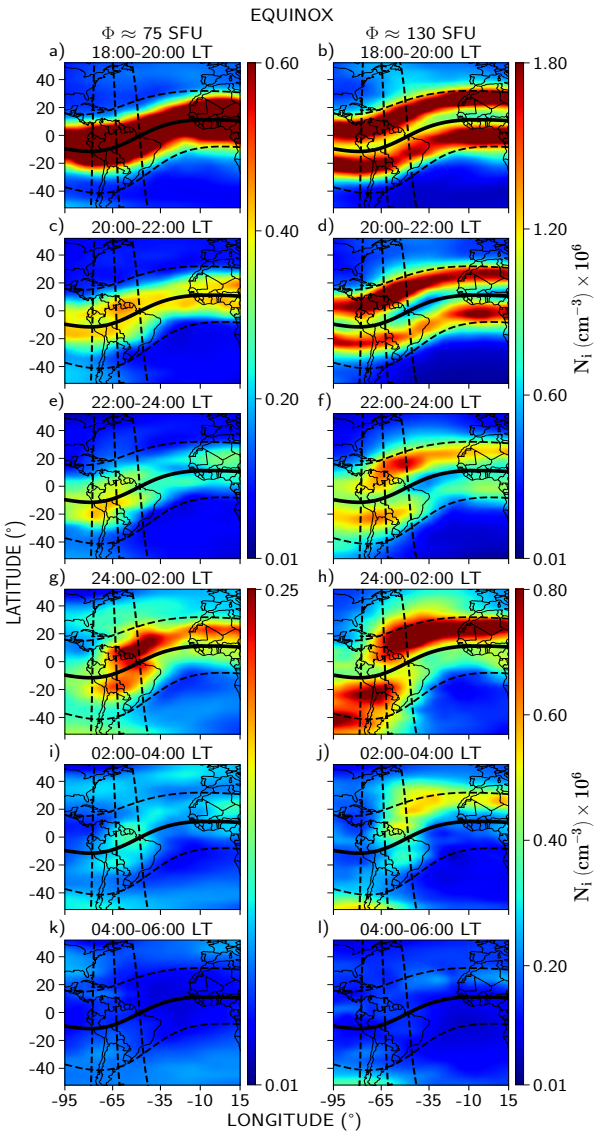

Figure 7. Same as Figure 6, but for the equinox.

a nearly constant longitude range from the nighttime until the early morning and contains the greatest densities from low- to mid-latitudes.

Equinox. The equinoctial data (Figure 7) shows both the Weddell Sea anomaly and the North Atlantic June solstice density enhancements appearing at 24:00-02:00 LT (Figures 7g-h), though less prominently. This is particularly the case for the WSA, in which only a weak anomaly is seen in the South Pacific. As is the case for the June solstice, from 20:00-22:00 LT to 02:00-04:00 LT the equinoctial northern hemisphere density enhancements are accompanied by density decreases in the conjugate hemisphere. Compared to the June solstice, the equinoctial North Atlantic MSNA is seen only until 02:00-04:00 LT, after which the anomaly is no longer clearly seen.

The MSNAs characteristics inferred from the FPMU data are consistent with those reported by Lin et al. (2010) and H. Liu et al. (2010), who suggested that these midlatitude structures are restricted to longitudes where the magnetic and geographic equa-

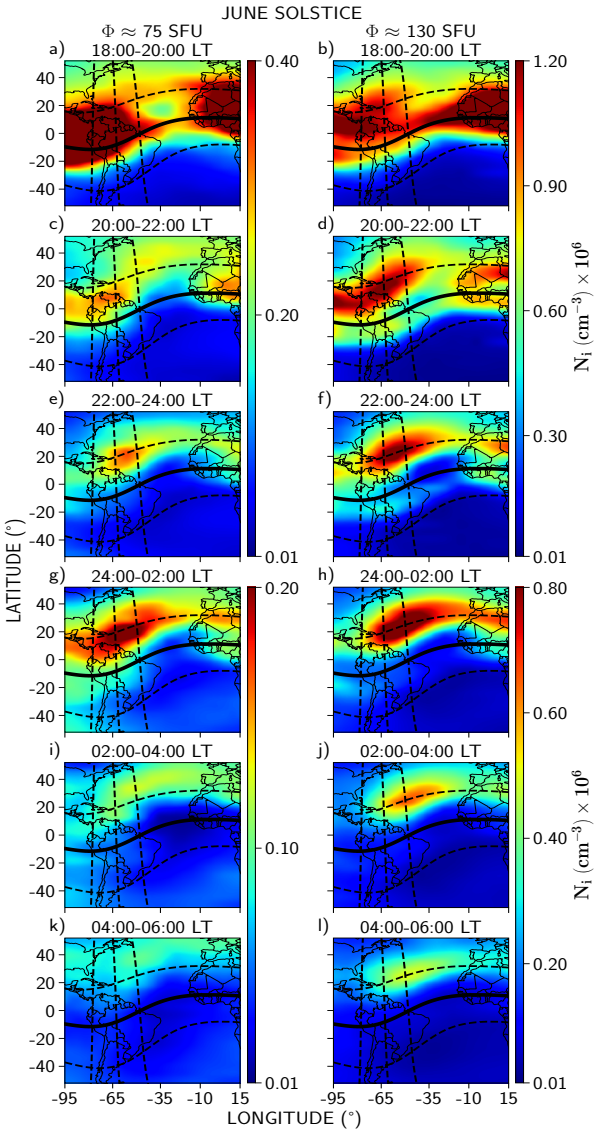

Figure 8. Same as Figure 6, but for the June solstice.

tors are apart from each other. Moreover, Figures 6 and 8 indicate that the December solstice WSA plasma density and its spatial coverage are greater than in the June solstice North Atlantic region, also in agreement with H. Liu et al. (2010). In our data, the WSA encompasses a very large longitude and latitude area, from the Australian to South Atlantic sectors (the total WSA area is not shown in Figure 6), whereas the North Atlantic structure in June solstice is seen restricted from Eastern Central America to Western Europe. This can be explained by the large declination angle near the South American anomaly, which produces a zonal wind more effective in the South Pacific than in the North Atlantic.

In contrast with previous results (e.g., Chen et al., 2012), the FPMU data show that the MSNAs during December and June solstice have similar local time occurrences. Additionally, our data show that both the WSA and the June density anomaly are stronger and have a longer lifetime during moderate solar flux conditions, which differs from the negative solar activity dependence suggested by Chen et al. (2012) and H. Liu et al. (2010).

These different results might be explained by our in-situ ion densities at 400 km, near hmF2 at night, where the MSNAs are expected to be more prominent (H. Liu et al., 2010). Many earlier studies used plasma densities from TEC and NmF2 measurements, which often do not correspond to the height of our in-situ plasma density data.

3.4.2 Plasma Depletion Bays

There is another feature clearly seen at the nighttime June solstice. Plasma depletion bays are observed almost at all local times shown in Figure 8. The PDBs appear as regions of depleted plasma density "curving in" to the northern hemisphere from the southern over North Atlantic longitudes. This feature is one of the South PDBs described by F.-Y. Chang et al. (2020). In the left panels of Figure 8, this depletion is seen from 18:00-20:00 LT, but only from 20:00-22:00 LT in the right panels, suggesting its earlier predominance during a low solar flux level. Our data shows that this feature appears at night during solstice months, consistent with previous studies (e.g., F.-Y. Chang et al., 2020). J.-Y. Liu et al. (2023) state that the number of PDBs can be affected by the observation altitude. Hence, at the ISS height, we only observe one PDB.

The equinox (Figure 7) shows a density depletion forming at 24:00-02:00 LT, seen until the early morning for both flux ranges. This depletion is located between South America and Africa, but it is not clear if it is associated with a plasma depletion bay, although there are similarities with this same phenomenon during the June solstice.

3.5 Relevant Atlantic and American Sectors Nighttime and Daytime Structures

The phenomena described in the previous sections highlighted the peculiarity of the Atlantic and American sectors. We proceed to examine some of their phenomena in more detail to investigate their evolution.

3.5.1 Nighttime

Figure 9 shows the density variation at 20:00-22:00 LT along the -5°, 10°, and 25° magnetic longitudes drawn in Figures 6-8. A clear longitudinal variation can be observed in the three seasons. During the December solstice, the strongest increase in the crest-to-trough density ratio with solar flux occurs along the 10° magnetic longitude line. The densities along the other two longitudes display well-defined crests for both fluxes. Additionally, the -5° and 10° lines show a density asymmetry with larger values in the northern crest. Comparing this result with those in Figures 5 and 6, we suggest that the asymmetry is a consequence of the EIA longitudinal variations.

The Weddell Sea anomaly significantly influences the December solstice densities in Figures 9a and 9b, as well as the equinoctial densities in Figure 9a, particularly at southern dip latitudes, with higher values toward the west. Hence, Figure 9 shows that the Weddell Sea anomaly is observed at 20:00-22:00 LT during the equinox for low, but not for moderate flux. The 10° magnetic longitude line displays an opposing behavior compared to the other two in Figure 9a during the equinox since it is the only one with a northern EIA crest greater than the southern. In Figure 9b, the three lines show well-developed and asymmetric EIA crests, with the northern having higher densities than the southern.

During the June solstice, Figure 9a shows only a single density peak at the -5° line, but strong asymmetries at 25° and 10° longitudes, with a much larger northern than southern crest. In fact, there is no southern crest at all at 10° longitude. In Figure 9b, the asymmetry for these two lines holds, but now the -5° also displays the same asymmetry between the southern and northern EIA crest. These equinox and June solstice asymme-

tries for both fluxes correspond to the northern hemisphere MSNA shown in Figures 7-8. As above-mentioned, the 10° magnetic longitude, which essentially crosses all of South America, is the one with the largest density variation with solar flux among all three seasons. Furthermore, it is evident from Figure 9 that the South American sector displays marked longitudinal plasma density variations.

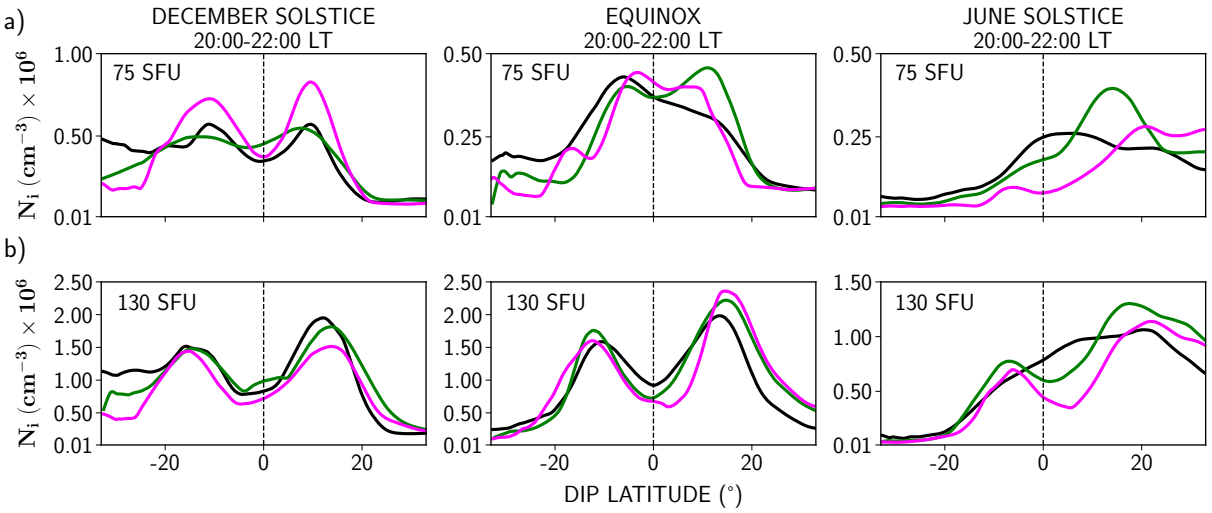

Figure 9. FPMU densities at 20:00-22:00 LT along the -5° (black), 10° (green), and 25° (pink) magnetic longitude lines for our a) low and b) moderate solar flux conditions.

3.5.2 Daytime

There is a pronounced feature in the daytime December solstice and equinox for both solar fluxes shown in Figures 1-2. A density bulge can be seen in the southern EIA crest in the -60° to 0° longitude sector from 12:00 to 16:00 LT. This bulge is identified as an increase in the latitudinal width or range of the South Atlantic EIA crest from 08:00 LT to 16:00 LT. Except for the work by H. Liu et al. (2010), which shows a similar bulge at 12:00 LT during the December solstice but does not mention it in the text, this is the first time this EIA bulge is examined in some detail along with a suggestion of its possible origin.

Figure 10 shows the local time evolution of the plasma density in the bulge region and along the 40° magnetic longitude lines (also drawn in Figures 1-2) during low and moderate solar flux levels for the December solstice and equinox and in three different local times prior to the ones presented in Figures 1-2: 06:00-08:00 LT, 08:00-10:00 LT and 10:00-12:00 LT. The 40° magnetic longitude line crosses the bulge region. The density variation in each field line was smoothed using a non-parametric fitting technique with a locally weighted smoothing regression algorithm. The 40° magnetic longitude lines were drawn in the June solstice maps in Figure 3 only for comparison since no bulge can be observed during this season.

December solstice displays the most distinctive bulge for both solar flux levels when compared to the equinoctial. This feature is more prominent in the moderate flux (Figures 10b, f, j) than in the low data (Figures 10a, e, i). At 06:00-08:00 LT, the Weddell Sea anomaly is still evident for all the maps at this local time period, except for the equinox during the low solar flux period. Most of the earlier studies cited in Section 3.4.1 observed the WSA until ∼04:00 LT. At 08:00-10:00 LT in Figure 10f, the WSA has moved north to lower latitudes. At 10:00-12:00 LT the December solstice enhancement moved north-

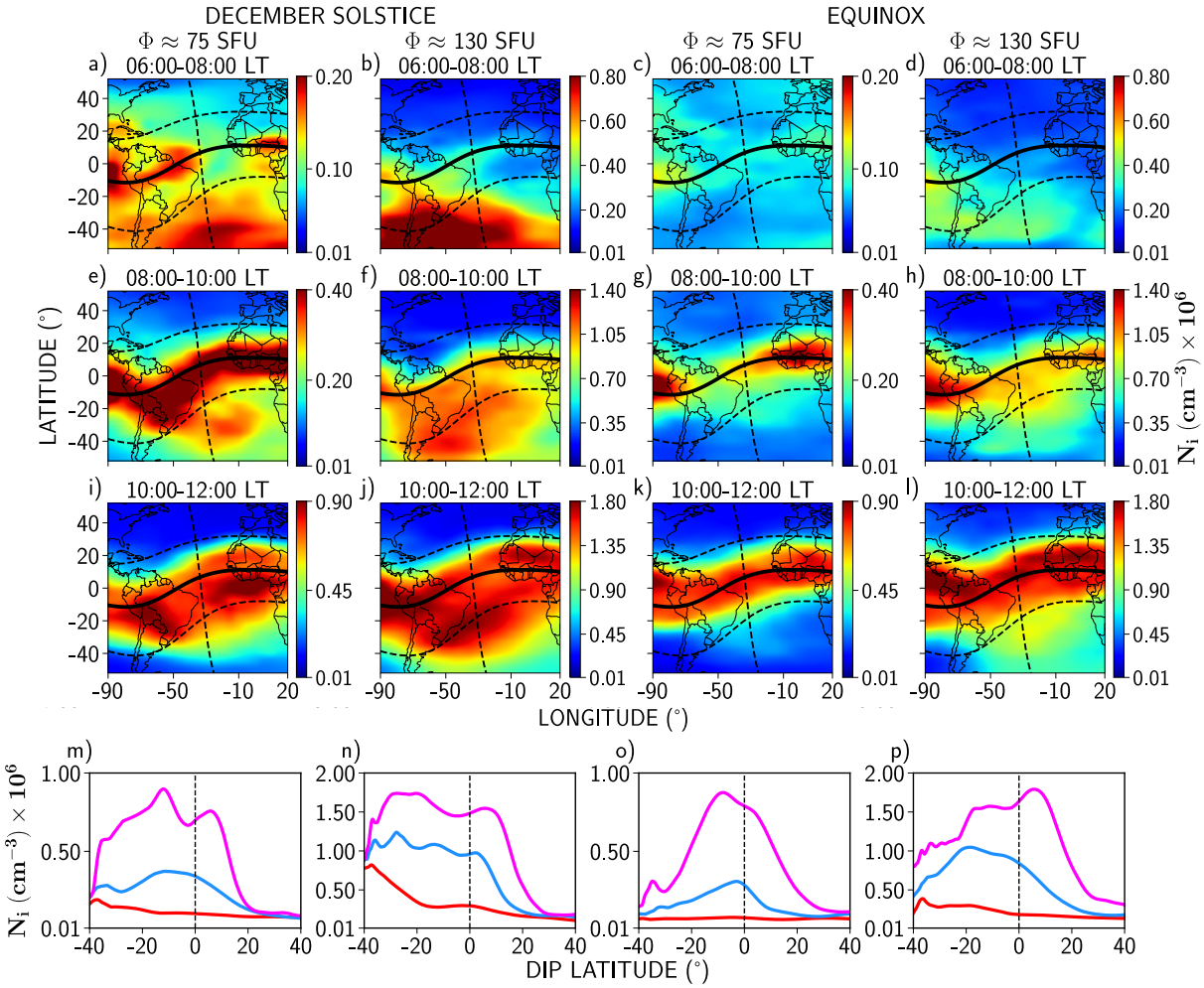

Figure 10. Local time evolution of the plasma density bulge region during December solstice (first and second columns) and equinox (third and fourth columns). The line plots in m-p show the plasma density variation along the 40° magnetic longitude line at 06:00-08:00 LT (red), 08:00-10:00 LT (blue), and 10:00-12:00 LT (pink) corresponding to columns in panels a-l.

ward (Figure 10j), merging with the EIA southern crest to form the bulge seen in Figure 1. The same process occurs during the equinox, but the bulge is less prominent. For $\Phi \approx 75$ sfu, the northern displacement of the WSA is less pronounced during both the December solstice and equinox, but a faint bulge can still be noticed in the EIA southern crest.

From the line plots perspective (Figures 10m-p), there is a density peak at approximately -38° dip latitude for both fluxes during the December solstice and only for $\Phi \approx 130$ sfu during the equinox. This peak becomes more intense and moves northward until it merges with the EIA southern crest, adding a bulge to it. From 08:00 LT to 12:00 LT, the asymmetry between the southern and northern crests is evident for both fluxes and seasons. We speculate that the bulge is associated with the WSA. The effect of the WSA is still observed during the early morning in our data and is responsible for the density peak at 06:00-08:00 LT in Figures 10m-n, p. Also, the bulge appears to be related to the WSA since it occurs in the region of greater separation between the geographic and magnetic equators, where the mid-latitude nighttime enhancements are preferred

to take place. Therefore, an equatorward meridional wind may oversee the WSA shift northwards. However, more detailed observations and numerical modeling are clearly necessary to determine the origin of this unusual plasma density feature.

4 Summary and Conclusions

We presented the first climatological study of mid- and low-latitude plasma densities derived from 12 years of FPMU measurements onboard the ISS during low and moderate solar flux conditions. Our daytime climatological results on the development, seasonal, and solar flux dependence of the EIA and location of their crests are consistent with earlier experimental results and can be largely explained as due to corresponding variations in the zonal electric fields and thermospheric neutral winds. Our middle and low-latitude daytime data also generally agree well with corresponding IRI ion densities. The FPMU evening and early night densities highlight the fundamental role of the PRE on the longitudinal variation of the crest-to-trough EIA anomaly crest ratios and of the meridional thermospheric winds on their hemispheric asymmetries. During this period the IRI density signatures strongly underestimate the moderate flux in-situ data for all three seasons.

We have shown a structuring in the daytime EIA southern crest during the December solstice and equinox that, to the best of the authors knowledge, was not noticed in previous studies. In the South Atlantic sector, this EIA latitudinal density bulge was stronger during moderate solar flux conditions. We suggest that this bulge is formed by the transport of plasma from the Weddell Sea anomaly. We showed that the ion density in the American and Atlantic sectors displays strong seasonal and longitudinal variations during the evening and the nighttime. This is particularly the case in the South American region. We also examined two midlatitude summer nighttime anomalies, the Weddell Sea anomaly in the South Pacific during the December solstice and the North Atlantic density enhancement during the June solstice. Our results indicate similarities between these anomalies. Both are stronger during a higher solar flux period and have all-night lifetimes at the ISS height, which is not consistent with earlier results, perhaps due to altitudinal effects. Additionally, since we have shown for the first time the WSA in the early morning, we discussed whether this supports its correlation with the density bulge in the EIA.

5 Open Research

The plasma densities used here are derived from FPMU telemetry at NASA Marshall Space Flight Center and archived at the publicly available NASA SPDF (Suggs & Koontz, 2021). The IRI-2020 model outputs used in this study are available for open access in the Zenodo repository at Laranja (2023).

Acknowledgments

The research at the Aeronautics Institute of Technology was supported by the Coordenação de Aperfeiçoamento de Pessoal de Nível Superior - Brazil (CAPES) – Financing Code 001 under the process 88881.676788/2022-01 and partially supported by projects 16/24970-7 by Fundação de Amparo à Pesquisa do Estado de São Paulo (FAPESP) and 305904/2019-1 by Conselho Nacional de Desenvolvimento Científico e Tecnológico (CNPq). The research at Utah State University was funded by NASA grants 80MSFC18C0010 and 80NSSC17K071.

References

Abdu, M. A., Bittencourt, J. A., & Batista, I. S. (1981). Magnetic declination control of the equatorial f region dynamo electric field development and spread f.

Journal of Geophysical Research: Space Physics, *86*(A13), 11443–11446. doi: 10.1029/JA086iA13p11443

Appleton, E. V. (1946). Two anomalies in the ionosphere. *Nature*, *157*(3995), 691–691. doi: 10.1038/157691a0

Bailey, G. J., Su, Y., & Oyama, K.-I. (2000). Yearly variations in the low-latitude topside ionosphere. In *Annales geophysicae* (Vol. 18, pp. 789–798). doi: 10.1007/s00585-000-0789-0

Balan, N., Bailey, G. J., Abdu, M. A., Oyama, K.-I., Richards, P., MacDougall, J., & Batista, I. S. (1997a). Equatorial plasma fountain and its effects over three locations: Evidence for an additional layer, the f 3 layer. *Journal of Geophysical Research: Space Physics*, *102*(A2), 2047–2056. doi: 10.1029/95JA02639

Balan, N., Liu, L., & Le, H. (2018b). A brief review of equatorial ionization anomaly and ionospheric irregularities. *Earth and Planetary Physics*, *2*(4), 257–275. doi: 10.26464/epp2018025

Balan, N., Otsuka, Y., Bailey, G., & Fukao, S. (1998). Equinoctial asymmetries in the ionosphere and thermosphere observed by the mu radar. *Journal of Geophysical Research: Space Physics*, *103*(A5), 9481–9495. doi: 10.1029/97JA03137

Balan, N., Otsuka, Y., & Fukao, S. (1997b). New aspects in the annual variation of the ionosphere observed by the mu radar. *Geophysical research letters*, *24*(18), 2287–2290. doi: 10.1029/97GL02184

Balan, N., Rajesh, P. K., Sripathi, S., Tulasi Ram, S., Liu, J.-Y., & Bailey, G. J. (2013). Modeling and observations of the north–south ionospheric asymmetry at low latitudes at long deep solar minimum. *Advances in Space Research*, *52*(3), 375–382. doi: 10.1016/j.asr.2013.04.003

Balan, N., Souza, J., & Bailey, G. (2018a). Recent developments in the understanding of equatorial ionization anomaly: A review. *Journal of Atmospheric and Solar-Terrestrial Physics*, *171*, 3–11. doi: 10.1016/j.jastp.2017.06.020

Balan, N., Thampi, S. V., Lynn, K., Otsuka, Y., Alleyne, H., Watanabe, S., ... Fejer, B. G. (2008). F3 layer during penetration electric field. *Journal of Geophysical Research: Space Physics*, *113*(A3). doi: 10.1029/2008JA013206

Bankov, L., Heelis, R. A., Parrot, M., Berthelier, J.-J., Marinov, P., & Vassileva, A. (2009). Wn4 effect on longitudinal distribution of different ion species in the topside ionosphere at low latitudes by means of demeter, dmsp-f13 and dmsp-f15 data. In *Annales geophysicae* (Vol. 27, pp. 2893–2902). doi: 10.5194/angeo-27-2893-2009

Barjatya, A., Swenson, C. M., Thompson, D. C., & Wright, K. H. (2009). Invited article: Data analysis of the floating potential measurement unit aboard the international space station. *Review of Scientific Instruments*, *80*(4). doi: 10.1063/1.3116085

Batista, I. S., Diogo, E. M., Souza, J. R., Abdu, M. A., & Bailey, G. J. (2011). Equatorial ionization anomaly: The role of thermospheric winds and the effects of the geomagnetic field secular variation. *Aeronomy of the Earth's Atmosphere and Ionosphere*, 317–328. doi: 10.1029/2008JA013089

Bilitza, D., Pezzopane, M., Truhlik, V., Altadill, D., Reinisch, B. W., & Pignalberi, A. (2022). The international reference ionosphere model: A review and description of an ionospheric benchmark. *Reviews of Geophysics*, *60*(4), e2022RG000792. doi: 10.1029/2022RG000792

Burns, A. G., Solomon, S. C., Wang, W., Qian, L., Zhang, Y., & Paxton, L. (2012). Daytime climatology of ionospheric nmf2 and hmf2 from cosmic data. *Journal of Geophysical Research: Space Physics*, *117*(A9). doi: 10.1029/2012JA017529

Burns, A. G., Zeng, Z., Wang, W., Lei, J., Solomon, S. C., Richmond, A., ... Kuo, Y.-H. (2008). Behavior of the f2 peak ionosphere over the south pacific at dusk during quiet summer conditions from cosmic data. *Journal of Geophysical*

Research: Space Physics, *113*(A12). doi: 10.1029/2008JA013308

Cai, X., Burns, A. G., Wang, W., Coster, A. J., Qian, L., Liu, J., ... McClintock, W. E. (2020). Comparison of gold nighttime measurements with total electron content: Preliminary results. *Journal of Geophysical Research: Space Physics*, *125*(9), e2019JA027767. doi: 10.1029/2019JA027767

Chang, F.-Y., Liu, J.-Y., Fang, T.-W., Rajesh, P. K., & Lin, C.-H. (2020). Plasma depletion bays in the equatorial ionosphere observed by formosat-3/cosmic during 2007–2014. *Journal of Geophysical Research: Space Physics*, *125*(9), e2019JA027501. doi: 10.1029/2019JA027501

Chang, L. C., Liu, H., Miyoshi, Y., Chen, C.-H., Chang, F.-Y., Lin, C.-H., ... Sun, Y.-Y. (2015). Structure and origins of the weddell sea anomaly from tidal and planetary wave signatures in formosat-3/cosmic observations and gaia gcm simulations. *Journal of Geophysical Research: Space Physics*, *120*(2), 1325–1340. doi: 10.1002/2014JA020752

Chen, C.-H., Saito, A., Lin, C.-H., & Liu, J.-Y. (2012). Long-term variations of the nighttime electron density enhancement during the ionospheric midlatitude summer. *Journal of Geophysical Research: Space Physics*, *117*(A7). doi: 10.1029/2011JA017138

Choi, J.-M., Lin, C.-H., Panthalingal Krishanunni, R., Park, J., Kwak, Y.-S., Chen, S.-P., ... Chang, M.-T. (2023). Comparisons of in situ ionospheric density using ion velocity meters onboard formosat-7/cosmic-2 and icon missions. *Earth, Planets and Space*, *75*(1), 15. doi: 10.1186/s40623-022-01759-3

Coffey, V. N., Wright, K. H., Minow, J. I., Schneider, T. A., Vaughn, J. A., Craven, P. D., ... Bui, T. H. (2008). Validation of the plasma densities and temperatures from the iss floating potential measurement unit. *IEEE transactions on plasma science*, *36*(5), 2301–2308. doi: 10.1109/TPS.2008.2004271

Dao, E., Kelley, M. C., Roddy, P., Retterer, J., Ballenthin, J., de La Beaujardiere, O., & Su, Y.-J. (2011). Longitudinal and seasonal dependence of nighttime equatorial plasma density irregularities during solar minimum detected on the c/nofs satellite. *Geophysical Research Letters*, *38*(10). doi: 10.1029/2011GL047046

Debchoudhury, S., Barjatya, A., Minow, J. I., Coffey, V. N., & Chandler, M. O. (2021). Observations and validation of plasma density, temperature, and abundance from a langmuir probe onboard the international space station. *Journal of Geophysical Research: Space Physics*, *126*(10), e2021JA029393. doi: 10.1029/2021JA029393

Debchoudhury, S., Barjatya, A., Minow, J. I., Coffey, V. N., & Parker, L. N. (2022). Climatology of deep o+ dropouts in the night-time f-region in solar minimum measured by a langmuir probe onboard the international space station. *Journal of Geophysical Research: Space Physics*, *127*(7), e2022JA030446. doi: 10.1029/2022JA030446

Eastes, R. W., Karan, D. K., Martinis, C., Daniell, R. E., Gan, Q., Burns, A. G., & McClintock, W. E. (2023). Gold observations of longitudinal variations in the nighttime equatorial ionization anomaly (eia) crests' latitudes. *Journal of Geophysical Research: Space Physics*, *128*(4), e2022JA031007. doi: 10.1029/2022JA031007

Fejer, B. G. (1991). Low latitude electrodynamic plasma drifts: A review. *Journal of Atmospheric and Terrestrial Physics*, *53*(8), 677–693. doi: 10.1016/0021-9169(91)90121-M

Fejer, B. G. (2011). Low latitude ionospheric electrodynamics. *Space Science Reviews*, *158*, 145–166. doi: 10.1007/s11214-010-9690-7

Fejer, B. G., Jensen, J. W., & Su, S.-Y. (2008). Quiet time equatorial f region vertical plasma drift model derived from rocsat-1 observations. *Journal of Geophysical Research: Space Physics*, *113*(A5). doi: 10.1029/2007JA012801

Fejer, B. G., & Maute, A. (2021). Equatorial ionospheric electrodynamics. *Iono-*

sphere dynamics and applications, 159–183. doi: 10.1002/9781119815617.ch9

Hanson, W., & Sanatani, S. (1971). Relationship between fe+ ions and equatorial spread f. *Journal of Geophysical Research*, *76*(31), 7761–7768. doi: 10.1029/JA076i031p07761

Hartman, W. A., Schmidl, W. D., Mikatarian, R., & Galkin, I. (2019). Correlation of irtam and fpmu data confirming the application of irtam to support iss program safety. *Advances in Space Research*, *63*(6), 1838–1844. doi: 10.1016/j.asr.2018.12.007

Heelis, R. A., Kendall, P., Moffett, R., Windle, D., & Rishbeth, H. (1974). Electrical coupling of the e-and f-regions and its effect on f-region drifts and winds. *Planetary and Space Science*, *22*(5), 743–756. doi: 10.1016/0032-0633(74)90144-5

Huang, C.-S., Rich, F. J., de La Beaujardiere, O., & Heelis, R. A. (2010). Longitudinal and seasonal variations of the equatorial ionospheric ion density and eastward drift velocity in the dusk sector. *Journal of Geophysical Research: Space Physics*, *115*(A2). doi: 10.1029/2009JA014503

Kelley, M. C. (2009). Dynamics and electrodynamics of the equatorial zone. In L. Shelton (Ed.), *The earth's ionosphere: Plasma physics and electrodynamics* (pp. 71–129). Cambridge, Massachusetts, USA: Academic press.

Khadka, S. M., Valladares, C. E., Sheehan, R., & Gerrard, A. J. (2018). Effects of electric field and neutral wind on the asymmetry of equatorial ionization anomaly. *Radio Science*, *53*(5), 683–697. doi: 10.1029/2017RS006428

Kumar, A., Chakrabarty, D., Pandey, K., Fejer, B., Sunda, S., Seemala, G., ... Yadav, A. (2021). Evidence for the significant differences in response times of equatorial ionization anomaly crest corresponding to plasma fountains during daytime and post-sunset hours. *Journal of Geophysical Research: Space Physics*, *126*(3), e2020JA028628. doi: 10.1029/2020JA028628

Laranja, S. R. (2023). Ion Density Climatology Based on FPMU Measurements on Board the International Space Station [Dataset]. Zenodo. Retrieved from `https://doi.org/10.5281/zenodo.8226439`

Li, G., Ning, B., Liu, L., Zhao, B., Yue, X., Su, S.-Y., & Venkatraman, S. (2008). Correlative study of plasma bubbles, evening equatorial ionization anomaly, and equatorial prereversal e× b drifts at solar maximum. *Radio Science*, *43*(04), 1–11. doi: 10.1029/2007RS003760

Lin, C.-H., Liu, C.-H., Liu, J.-Y., Chen, C.-H., Burns, A. G., & Wang, W. (2010). Midlatitude summer nighttime anomaly of the ionospheric electron density observed by formosat-3/cosmic. *Journal of Geophysical Research: Space Physics*, *115*(A3). doi: 10.1029/2009JA014084

Lin, C.-H., Liu, J.-Y., Cheng, C.-Z., Chen, C.-H., Liu, C.-H., Wang, W., ... Lei, J. (2009). Three-dimensional ionospheric electron density structure of the weddell sea anomaly. *Journal of Geophysical Research: Space Physics*, *114*(A2). doi: 10.1029/2008JA013455

Lin, C.-H., Wang, W., Hagan, M. E., Hsiao, C., Immel, T., Hsu, M., ... Liu, C.-H. (2007). Plausible effect of atmospheric tides on the equatorial ionosphere observed by the formosat-3/cosmic: Three-dimensional electron density structures. *Geophysical Research Letters*, *34*(11). doi: 10.1029/2007GL029265

Liu, H., Thampi, S. V., & Yamamoto, M. (2010). Phase reversal of the diurnal cycle in the midlatitude ionosphere. *Journal of Geophysical Research: Space Physics*, *115*(A1). doi: 10.1029/2009JA014689

Liu, J., Wang, W., Burns, A. G., Solomon, S. C., Zhang, S., Zhang, Y., & Huang, C.-S. (2016). Relative importance of horizontal and vertical transports to the formation of ionospheric storm-enhanced density and polar tongue of ionization. *Journal of Geophysical Research: Space Physics*, *121*(8), 8121–8133. doi: 10.1002/2016JA022882

Liu, J.-Y., Kan, K.-W., Chao, C.-K., & Chang, F.-Y. (2023). Nighttime wavenumber-four and plasma depletion bays observed by formosat-5/aip,

icon/ivm, and cosmic-2/ro data. *Advances in Space Research*. doi: 10.1016/j.asr.2023.04.047

Liu, J.-Y., Lin, C.-H., Lin, C.-Y., Lee, I.-T., Sun, Y.-Y., Chen, S.-P., ... others (2022). Retrospect and prospect of ionospheric weather observed by formosat-3/cosmic and formosat-7/cosmic-2. *Terrestrial, Atmospheric and Oceanic Sciences*, *33*(1), 20. doi: 0.1007/s44195-022-00019-x

Luan, X., & Solomon, S. C. (2008). Meridional winds derived from cosmic radio occultation measurements. *Journal of Geophysical Research: Space Physics*, *113*(A8).

Luan, X., Wang, P., Dou, X., & Liu, Y. C.-M. (2015). Interhemispheric asymmetry of the equatorial ionization anomaly in solstices observed by cosmic during 2007–2012. *Journal of Geophysical Research: Space Physics*, *120*(4), 3059–3073. doi: 10.1002/2014JA020820

Newheart, A. M., Sazykin, S., Coffey, V. N., Chandler, M. O., Coster, A. J., Fejer, B. G., ... Swenson, C. M. (2022). Observations of night-time equatorial ionosphere structure with the fpmu on board the international space station. *Journal of Geophysical Research: Space Physics*, *127*(11), e2022JA030373. doi: 10.1029/2022JA030373

Penndorf, R. (1965). The average ionospheric conditions over the antarctic. *Geomagnetism and Aeronomy: studies in the ionosphere, geomagnetism and atmospheric radio noise*, *4*, 1–45. doi: 10.1029/AR004p0001

Rishbeth, H. (1981). The f-region dynamo. *Journal of Atmospheric and Terrestrial Physics*, *43*(5-6), 387–392. doi: 10.1016/0021-9169(81)90102-1

Rishbeth, H., & Garriott, O. K. (1969). Introduction to ionospheric physics. *Introduction to ionospheric physics*.

Savitzky, A., & Golay, M. J. (1964). Smoothing and differentiation of data by simplified least squares procedures. *Analytical chemistry*, *36*(8), 1627–1639. doi: 10.1021/ac60214a047

Scherliess, L., & Fejer, B. G. (1999). Radar and satellite global equatorial f region vertical drift model. *Journal of Geophysical Research: Space Physics*, *104*(A4), 6829–6842. doi: 10.1029/1999JA900025

Stolle, C., Lühr, H., & Fejer, B. G. (2008). Relation between the occurrence rate of esf and the equatorial vertical plasma drift velocity at sunset derived from global observations. In *Annales geophysicae* (Vol. 26, pp. 3979–3988). doi: 10.5194/angeo-26-3979-2008

Suggs, R., & Koontz, S. (2021). ISS Floating Potential Measurement Unit (FPMU), 1 s Data [Dataset]. NASA Space Physics Data Facility. Retrieved 01/15/2023, from `https://spdf.gsfc.nasa.gov/pub/data/international_space_station_iss/sp_fpmu/`

Tulasi Ram, S., Su, S.-Y., & Liu, C.-H. (2009). Formosat-3/cosmic observations of seasonal and longitudinal variations of equatorial ionization anomaly and its interhemispheric asymmetry during the solar minimum period. *Journal of Geophysical Research: Space Physics*, *114*(A6). doi: 10.1029/2008JA013880

Wan, W., Liu, L., Pi, X., Zhang, M.-L., Ning, B., Xiong, J., & Ding, F. (2008). Wavenumber-4 patterns of the total electron content over the low latitude ionosphere. *Geophysical Research Letters*, *35*(12). doi: 10.1029/2008GL033755

Whalen, J. A. (2004). Linear dependence of the postsunset equatorial anomaly electron density on solar flux and its relation to the maximum prereversal e× b drift velocity through its dependence on solar flux. *Journal of Geophysical Research: Space Physics*, *109*(A7). doi: 10.1029/2004JA010528

Wharton, L., Spencer, N., & Brinton, H. (1980). Correlations between neutral meridional winds and ion densities observed on ae-e. *Journal of Geophysical Research: Space Physics*, *85*(A9), 4653–4657. doi: 10.1029/JA085iA09p04653

Xiong, C., Lühr, H., & Ma, S. (2013). The magnitude and inter-hemispheric asym-

metry of equatorial ionization anomaly-based on champ and grace observations. *Journal of Atmospheric and Solar-Terrestrial Physics*, *105*, 160–169. doi: 10.1016/j.jastp.2013.09.010

Yang, T.-Y., Park, J., Kwak, Y.-S., Oyama, K.-I., Minow, J. I., & Lee, J. (2020). Morning overshoot of electron temperature as observed by the swarm constellation and the international space station. *Journal of Geophysical Research: Space Physics*, *125*(2), e2019JA027299. doi: 10.1029/2019JA027299

Zeng, Z., Burns, A. G., Wang, W., Lei, J., Solomon, S., Syndergaard, S., ... Kuo, Y.-H. (2008). Ionospheric annual asymmetry observed by the cosmic radio occultation measurements and simulated by the tiegcm. *Journal of Geophysical Research: Space Physics*, *113*(A7). doi: 10.1029/2007JA012897